Energy 282 (2023) 128763

Contents lists available at ScienceDirect

Energy

journal homepage: www.elsevier.com/locate/energy

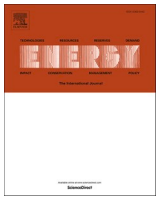

Assessment of single rotor expander-compressor device in combined organic Rankine cycle (ORC) and vapor compression refrigeration cycle (VCR)

Saif Alshammari [a,b], Sambhaji T. Kadam [a], Zhibin Yu [a,*]

[a] James Watt School of Engineering, University of Glasgow, Glasgow, G12 8QQ, UK
[b] Department of Mechanical Engineering, College of Engineering, Jouf University, Sakakah 72388, Saudi Arabia

ARTICLE INFO

Keywords:
Organic Rankine cycle
Vapor compression refrigeration cycle
Expander-compressor
Energy
Exergy

ABSTRACT

An environmental degradation due to consumption of fossil fuel based high grade energy releasing greenhouse gases is a pressing issue around the world. The use of low-grade heat from renewable energy sources using organic Rankine cycle is an attractive solution to reduce of emission of greenhouse gases and protect the environment. This paper investigates the potential of a new single rotor expander-compressor device in a combined Vapor Compression Refrigeration (VCR) cycle and an organic Rankine cycle (ORC). The numerical model of combined ORC-VCR is developed and validated. The thermal performance of combined cycle has been evaluated under the influence of evaporation temperature of ORC (62.75 °C–89.7 °C) and VCR (−20 °C–5 °C), condensation temperature of ORC (20 °C–45 °C) and rotor speed (500–3000 rpm) at a constant hot source (water) temperature of 95 °C. The maximum cooling effect, heat-to-cooling efficiency, and exergy efficiency achieved are found to be 5.38 kW, 56% and 63% when the evaporation temperature of ORC and VCR is 62.75 °C and −5 °C, and condensation temperature of ORC is 20.5 °C. Moreover, cooling effect increases linearly with the rotor speed, however, the heat-to-cooling efficiency and exergy efficiency are not affected by the rotor speed.

1. Introduction

The increasing consumption of fossil fuels and associated emissions of greenhouse gases is a worldwide alarming and threatening challenge due to increasing level of global warming effect [1]. As a result, the average surface air temperature has continued to rise, with a dramatic increase of more than 0.5 °C since 1970s recent decades [2]. This scenario demands more refrigeration and air conditioning systems to be used consuming 20% of fossil-based electricity worldwide, and anticipated consumption will reach 7500 TWh by 2050 compared to 2018 (3900 TWh) [3,4]. Additionally, leakage of refrigerants into the atmosphere further increases global warming. This complex interdependence between fossil fuel use, greenhouse gas emissions, and refrigeration and air conditioning, however, poses a potentially harmful threat to the environment. Recognition this, the Paris Agreement entered into force in November 2016 with the aim of limiting global warming below 2 °C in the context of sustainable development [5].

Consequently, renewable low-temperature energy sources such as solar, biomass, geothermal or waste heat, which would otherwise be wasted, complement social and environmental sustainability, attracting researchers. The low-grade temperature thermal energy can be harness by integrating with absorption refrigeration system in cooling application and organic Rankine cycle for cooling and/or power generation [6,7]. The former refrigeration system is only suitable for large-scale application due to its bulky size, operational complexity with low thermal efficiency. However, the organic Rankine cycle (ORC) is an emerging technology that shows significant potential for converting low-temperature heat sources into useful work [8–10] and making them suitable for small-scale application. Boiling organic liquids (refrigerants) at low temperatures enables heat recovery from low temperature energy sources [11].

The refrigerant used in a low temperature heat recovery must have low boiling temperature and latent heat of evaporation [12]. Li et al. [13] investigated performance of ORC-VCR system using different refrigerants. They observed that R134a exhibits better thermal performance compared to R22, R600 and concluded that turbine inlet pressure, heat source temperature and condensation temperature have dominating influence on the system performance. Li et al. [14] observed

* Corresponding author.
E-mail address: Zhibn.Yu@glasgow.ac.uk (Z. Yu).

https://doi.org/10.1016/j.energy.2023.128763
Received 20 January 2023; Received in revised form 3 May 2023; Accepted 13 August 2023
Available online 17 August 2023

that butane is a potential working fluid among propane, isobutane and propylene in ORC-VCR system. Kim and Perez-Blanco [15] studied ORC-VCR operated using R143a, R22, R134a, R152a, propane, ammonia, isobutane, and butane and concluded that different refrigerant exhibits better performance over other under different operating conditions. Nasir and Kim [16] identified that R134a and Isobutane are the best combination for ORC and VCR for domestic system among R245fa, R123, R134a, R1234yf, R1234ze (E), Butane and Isobutane, respectively. Saleh [17] concluded that R602 exhibits better ORC-VCR system performance with attaining highest COP of 0.99 and maximum exergy efficiency of 53.8% among many hydrocarbons, hydrofluorocarbons, fluorocarbons, hydrofluoroethers, and hydrofluoroolefins. Similarly, Xia et al. [18] and Ashwni et al. [19] observed that R602 is an optimal refrigerant in ORC-VCR application, while R1234yf shows worst performance.

Several efforts have been made to explore various aspects of ORC under the use of different types energy sources [20]. Askari-Asli Ardeh et al. [21] studied an ORC system driven by solar energy and observed that the maximum cycle efficiency can reach up to 35% and the lowest payback period is 8.79 years. Ziółkowski et al. [22] observed that the thermal and exergy efficiency of an ORC operated by a geothermal heat source at 120 °C was 10.5% and 29%, respectively. Rijpkema et al. [23] experimentally evaluated the performance of an ORC recovering heat from engine coolant at 92 °C and found that heat recovery up to 1.3% is possible using a high efficiency pump and expander. Dai et al. [24] used a thermal energy source with a temperature of 145 °C as input to an ORC and observed the optimum cycle efficiency to be around 12%. Liu et al. [25] numerically investigated the ORC considering waste heat and concluded that the highest efficiency achieved was 6.47% when the heat source temperature was 200 °C. Shao et al. [26] experimentally obtained an efficiency of 5.5%, while the heat source temperature was 140 °C. An ORC driven by a heat source at 150 °C is experimentally evaluated by Miao et al. [27] indicates that a cycle efficiency of 6.1% can be achieved.

An ORC system can be connected to an electric generator to produce electricity and/or directly drive the compressor of a vapor compression refrigeration (VCR) system to produce cooling effect [28,29]. Prigmore and Barber [30] developed and demonstrated a 1-kW solar-powered ORC system to electrify and/or drive a 3-ton air condition unit. An ORC uses R113, while an air conditioner works with R12 and a solar collector providing hot water at 102 °C. They found that considering 30% solar collector efficiency of, the coefficient of performance and system thermal ratio of the combined Rankine/air conditioning system are 0.71 and 0.21, respectively. Lior [31] studied a solar powered combined ORC-VCR cycle for cooling and heating applications. They revealed that the system can save up to 60% of energy compared to an electrically powered system with the same heating and cooling requirements. Wang et al. [32] observed that the overall COP of an integrated ORC-VCR cycle can reach 0.66 under extreme conditions. Chahartagi et al. [33] carried energy and exergy analysis of combined cooling, heating and power generation system and observed that the overall increase in energy efficiency of the entire system is 57%. Aphornratana and Sriveerakul [34] evaluated the performance of a vapor compression refrigeration cycle operated by a heat-driven ORC, in which both cycles share the same condenser and use the same working fluid (R134a and R22). The results show that the overall COP can reach up to 0.6 when both cycles are operated with R22. They further suggested that the ratio of the expander piston area to the compressor piston area strongly influences the overall COP of the system. Mahmoudan et al. [35] presented a combined ORC-VCR connected to steam Rankine turbine and a gas turbine to increase the efficiency of the cogeneration system. The results showed that the system could produce 303.8 kW of cooling effect. Similarly, Liang [36] experimentally studied the combined ORC-VCR to generate the refrigerating effect using low-grade temperature heat source using R245fa and R134a, respectively. The two cycles were coupled using a belt transmission unit and the heat source temperature was 95 °C. The results show that the system can produce 1.8 kW of refrigeration effects at – 4 °C while the overall performance can reach 0.18.

Fewer literature is available pertinent to experimental assessment of single rotor expander-compressor in ORC-VCR applications [37]. Wang et al. [38] experimentally demonstrated a new configuration of an ORC-VCR system using a scroll type of expander to drive a scroll type of compressor and an efficient microchannel heat exchanger. They concluded that the use of scroll expander and compressor facilitates high performance with reduced size and weight of system. Garland et al. [39] developed a prototype of ORC-VCR using magnetic coupling centrifugal turbine and compressor. The system operates using low-grade waste heat source at 106 °C and produces 250 kW of cooling. Similarly, Grauberger et al. [40] experimentally demonstrated the performance of an ORC-VCR system (264 kW) using a direct coupled centrifugal turbine and compressor.

The above lietrature represents the potential of the organic Rankine cycle in operating a vapor compression refrigeration system by direct coupling to drive compressor. In direct coupling either the expander shaft and the compressor shaft are connected through the transmission unit or both the expander and compressor are mounted on a common shaft. The latter arrangement may be more effective as the former may lead to transmission losses, balancing problems and additional system complexicity and cost. These issues can undermine the reliability of ORC. Liang [37] observed that the ORC-VCR system with a belt transmission unit has better performance and higher reliability than the common shaft arrangement. However, this discrepancy can be attributed to the consideration of the different working fluid in ORC under belt transmission (R245ca) and common shaft (R1233zd), which have different evaporation pressure.

Conventionally, in a common shaft expander-compressor arrangement, the compressor and expander are enclosed in separate casing. This presents a unique opportunity to improve the compression and expansion process to further improve thermal efficiency of the ORC-VCR system by reducing thermal losses. Thermodynamically, the expansion process prefers to be heated, while a compression process prefers to be cooled [41,42]. In a conventional vapor compression system, the heat of compression is transferred to the refrigerant raising the discharge temperature. This leads to an increase in specific volume at discharge and the compressor consumes more power due to isentropic compression. In contrast, the expansion in the conventional expander of ORC should be heated facilitating more power generation.

Changes in one component of the system can significantly affect the thermal performance of the entire system. Therefore, common shaft expander-compressor technology enclosed in a single casing should be exploited to further improve the expansion and compression processes of the ORC-VCR system. Recently, Jiang et al. [43] experimentally investigated a single rotor volute type expander-compressor enclosed in a single casing and concluded that the system can achieve good efficiency and stability. In this context, this paper addresses the potential of a new single rotor expander-compressor in which one side acts as expander while the other acts as a compressor enclosed in a single casing used in ORC-VCR applications. In the new expander-compressor, the heat of compression from the compressor side can be used on the expansion side, resulting in improved efficiency of both expansion and compression processes. Hence, the resulting new ORC-VCR system can be more efficient because the heat conduction within the device will benefit both expansion and compression processes than conventional ORC-VCR system with separate compressor and expander.

Additionally, this new device eliminates the need for a generator to convert mechanical power to electricity and an electrical motor to convert electricity to mechanical power, thereby increasing energy efficiency. Overall, the new device can offer improved compression and expansion processes, enhanced system efficiency, overall compactness and ultimately systems cost-effectiveness. However, the use of similar device for ORC-VCR systems with conventional refrigerants has not been

explored. A new single rotor expander-compressor in air cycle for cooling application has been studied by Fenton et al. [44] and Subert et al. [45]. They concluded that the device has the potential to overcome the performance limitations of conventional air cycles. Furthermore, Zhang et al. [46] reported based on experimental results that isentropic efficiency of the same device can reach 80%.

The aim of this paper is to numerically investigate the potential of a new device in an integrated ORC-VCR from the perspective of first and second law efficiency. A numerical model of the ORC-VCR cycle has been developed using ASPEN Plus and both the new single rotor expander-compressor device and the ORC-VCR system have been validated by comparing with previously published experimental data. The thermal performance of the ORC-VCR system with the new device is investigated under various system parameters such as expander inlet pressure, shaft speed, ORC evaporation and condensation temperatures. Parametric analysis provides a better understanding of the system parameters on the ultimate thermal performance of the entire ORC-VCR system. Heat-to-cooling efficiency is used as an energy indicator and overall exergy efficiency is used as an exergy indicator.

2. Materials and methodology

Fig. 1 presents the procedure followed in the present study. First, model is developed and validated for new device considering the air cycle and then complete ORC-VCR system is modeled and validated, as discussed in validation sections.

2.1. New single rotor expander-compressor

The new single rotor expander-compressor device is a positive displacement device consisting of four chambers mounted on a common spherical rotor and enclosed in a single casing. Fig. 2 shows the internal arrangement of the new device, which consists of two symmetrical halves (side A and side B) that act as expander and compressor and vice versa. Each half consists of a pair of double acting chambers as suction chamber and discharge chamber; i.e. suction port A, discharge port A, suction port B, and discharge port B. The displacement of side A is 15.7 cm^3 and that of side B is 23 cm^3. The chamber on each side rotates with the rotor and are designed in such a way that the rotation of the rotor properly opens and closes the inlet port and outlet port on both sides, enabling precise valveless operation of the device.

During 180° rotation, the two chambers on opposite sides (i.e. suction port A and suction port B) allow suction of the working fluid while the respective partner chambers compress and displace the working fluid through the discharge port (i.e. discharge port A and discharge port B). Fluid sealing is achieved very closely and thus the fluid from side A perfectly sealed from side B and vice versa and in the suction and discharge chambers of the same side. Detailed information about the device is available in Refs. [44–46].

2.2. Combined ORC-VCR system description

Fig. 3 shows a schematic diagram of the ORC and VCR interconnected by a new single rotor expander-compressor device. One side of the device acts as an expander in the ORC, while the other side is the compressor of the VCR. ORC consists of pump (PUMP), evaporator (EVAORC), expander (EXPANDER) and condenser (CONDORC). The liquid phase working fluid is pumped into the evaporator of the ORC, where it is boiled until completely vaporized and then passes through the expander imparting work and finally enters the condenser of the ORC to liquify.

VCR cycle consists of evaporator (EVAVCR), compressor (COMPRESO), condenser (CONDVCR), and expansion valve (EXPV). The vapor phase working fluid is compressed by the compressor which receives power from the expander of the ORC and condenses in the condenser, then expands to lower its temperature and finally evaporates completely in the evaporator. The work produced by the expander of ORC is fed directly to the compressor of VCR as they share the same shaft. Fig. 4 Presents corresponding P-h diagram. Two separate pressure-enthalpy envelopes are presented because two different working fluids are used in the present paper. The work generated by process 2–3 of the ORC is supplied to drive the compressor (process 8–5') of the VCR.

2.3. ORC-VCR model development

The model of ORC-VCR is developed in ASPEN PLUS® process simulator (V12.1) [47] as presented in Fig. 2. R245fa is used as the working fluid for ORC while R134a is the working fluid for VCR and water is the cooling medium. Table 1 presents the general properties of both refrigerants under consideration. Thermodynamic and transport properties are derived using the inbuilt REFPROP model as it is suitable for the fluids under consideration (i.e., R245fa, R134a and water). All heat exchangers, except evaporator of the VCR, are considered counter-flow configurations and are modeled using HeatX model, which is suitable for zone analysis of single-phase and two-phase flow. A list of all the operational units presented in Fig. 2 and corresponding ASPEN Plus models adopted from its library are presented in Table 2. Table 2 also compiles the input requirements under consideration and their ranges for each component of the ORC-VCR unit presented in Fig. 2.

The mass flow rates for ORC and VCR are obtained by eq. (1) and eq. (2) respectively. Using the chamber volume of the expander (V_E) and compressor (V_C) in the device, with assuming 100% volumetric efficiency [46], the following equations apply:

$$\dot{m}_{ORC} = \rho_2 N V_E \omega / 60 \tag{1}$$

$$\dot{m}_{VCR} = \rho_8 N V_C \omega / 60 \tag{2}$$

Where N is equal to 2 as one complete cycle is of 180° and ω is the shaft speed in rpm. The efficiency of the combined system is presented by heat to cooling efficiency (η_{H-C}) as shown by Eq. (3) [36].

$$\eta_{H-C} = \frac{Q_{eva,VCR}}{Q_{eva,ORC}} \tag{3}$$

Overall exergy of the system is estimated using Eq. (4) [17]. The exergy destruction occurred within the system is considered and the effect of the outside variable such as cooling water and source temperature are neglected to check feasibility of the device [17].

$$\eta_{oval-ex} = \frac{\dot{E}_{cooling}}{\dot{E}_{in}} \tag{4}$$

Where $\dot{E}_{cooling}$ is exergy destruction across the evaporator of the VCR system and $\dot{E}_{in}$ is the total exergy destruction across the evaporator of the ORC and the pump input power.

$$\dot{E}_{cooling} = \dot{E}_8 - \dot{E}_7 \tag{5}$$

$$\dot{E}_{in} = \dot{E}_2 - \dot{E}_1 + \dot{W}_{ORC-pump} \tag{6}$$

Where $\dot{E}$ is the exergy flow of the refrigerants and subscripts 1, 2, 7, and 8 denotes stream as presented in Fig. 2. The exergy flow is calculated using the following Eq. (7) [49].

$$\dot{E}_i = \dot{m}_{wf}[(h_i - h_0) - T_0(s_i - s_0)] \tag{7}$$

Where i is the stream number, i.e., subscripts 1, 2, 7, and 8, and T_0 is the dead state temperature in K.

2.4. Model validation

The validation is conducted in two steps, first is the validation of the single rotor expander-compressor device and second is the validation of

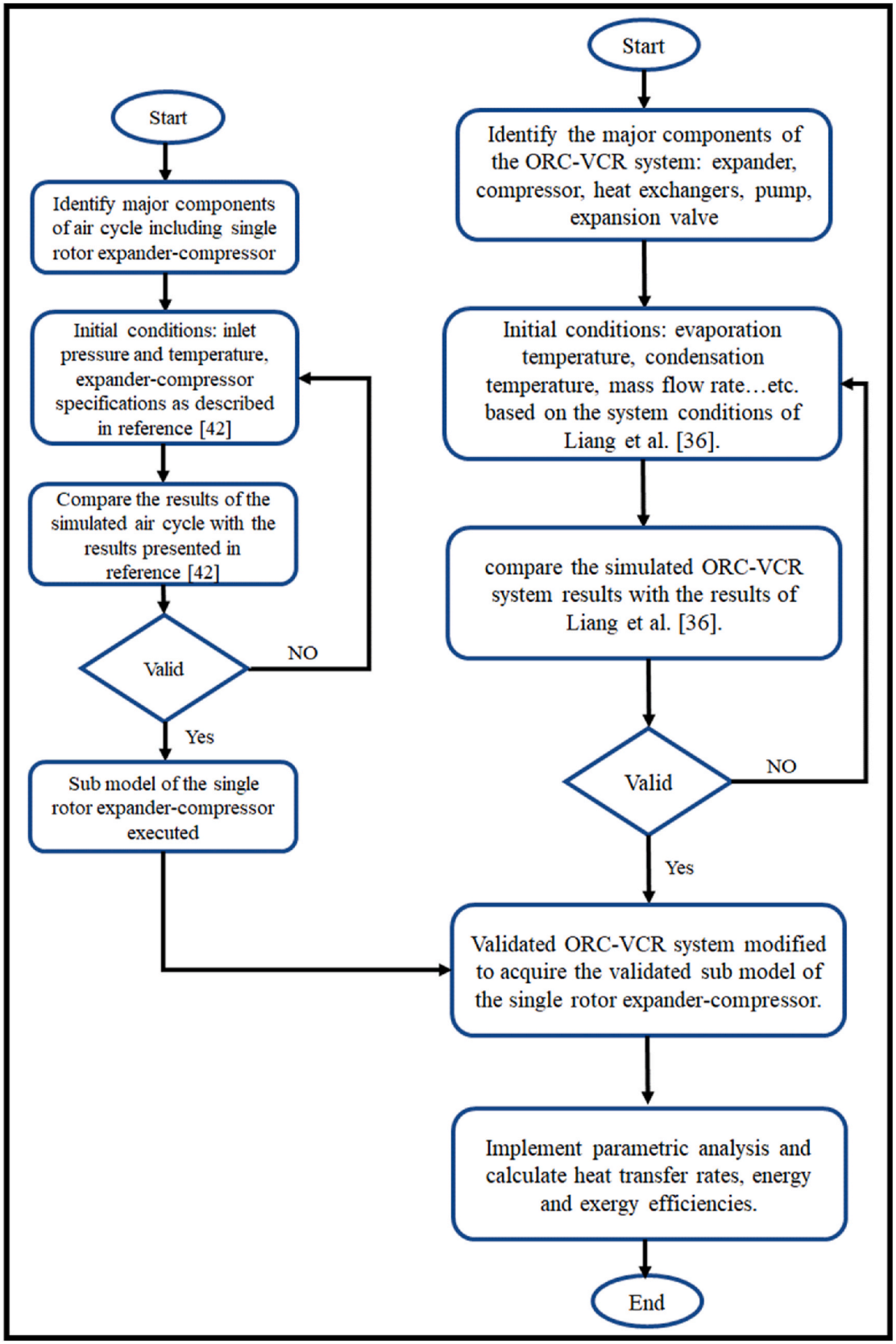

Fig. 1. Flowchart of procedure followed in ORC-VCR simulation and validation.

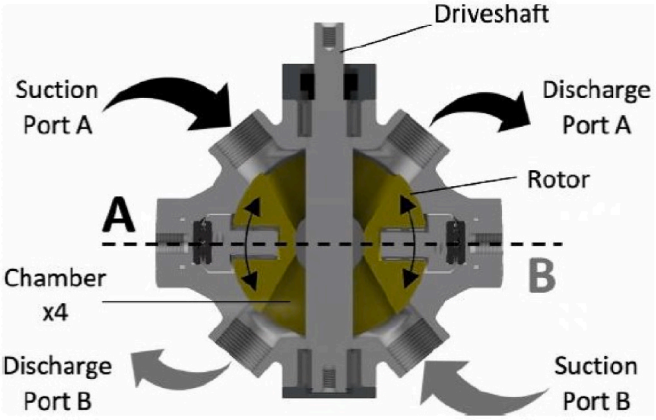

Fig. 2. New single rotor expander-compressor device (Fenton et al. [44]).

complete ORC-VCR system with experimental data. The validation procedure is presented in Fig. 6.

2.4.1. Validation of single rotor expander-compressor

To ensure the accuracy of the numerical simulation, a single rotor expander-compressor system presented in Fig. 5(a) is used as a reference system for validation [44]. They used air as the working fluid to enter the expander at 25 °C and 1 bar and expands to 0.6 bar and the corresponding temperature is −8 °C. The speed varies between 500 rpm and 3000 rpm while keeping inlet and outlet conditions the same. The resulting mass flow rate of the received air is compared with data of reference data [44] and presented with respect to shaft speed in Fig. 5 (b). The results show a particularly good correlation between the experimental and simulation results with a maximum deviation of less than 1%.

2.4.2. Validation of ORC-VCR system

After validating the new device, the numerical model of the complete ORC-VCR is developed and validated against the experimental results of Liang et al. [36]. They used two separate new devices connected by a belt drive mechanism which has a speed ratio of 1.71 to transmit the mechanical power from the ORC system to the VCR as shown in Fig. 6 (a).

In their study, the amount of work produced by the expander is not same as that of the work supplied to the compressor due to losses in the belt drive. This transmission losses are accounted by relating expander work and compressor work in the model. Fig. 6(b) presents a comparison between the present numerical model of the ORC-VCR system and the experimental results under different ORC mass flow rates. It is observed that the numerical simulation results show good agreement with the experimental data with a maximum deviation of about 5.6%. In current analysis, the model presented in Fig. 6(a) is modified by assuming that the work developed by the expander is fed completely to the compressor of the VCR.

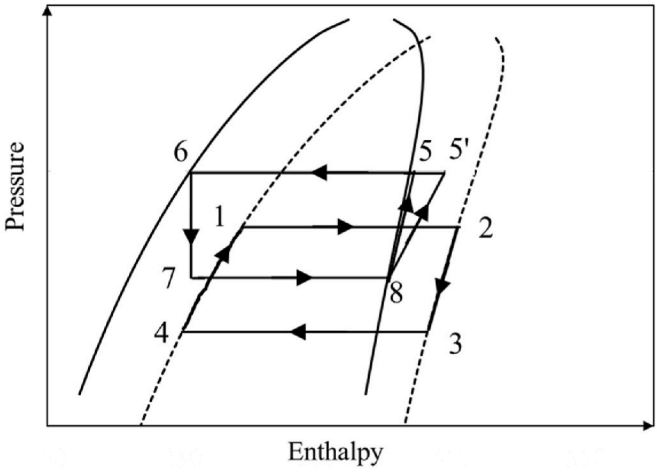

Fig. 4. Pressure-enthalpy diagram of current ORC-VCR system. Cycle 4-1-2-3 is ORC cycle and cycle 8-5-6-7 is VCR cycle.

Table 1
Refrigerants with environmental, health and safety properties.

Refrigerants	Atmospheric lifetime (years)	ODP[a]	GWP[a]	ASHRAE safety group[a]	ASHRAE Flammability[a]
R245fa	7.7	0	858	B1	No
R134a	14	0	1430	A1	No

[a] ASHRAE Handbook, Fundamentals (SI Edition), 2017, Chapter 29, Atlanta.

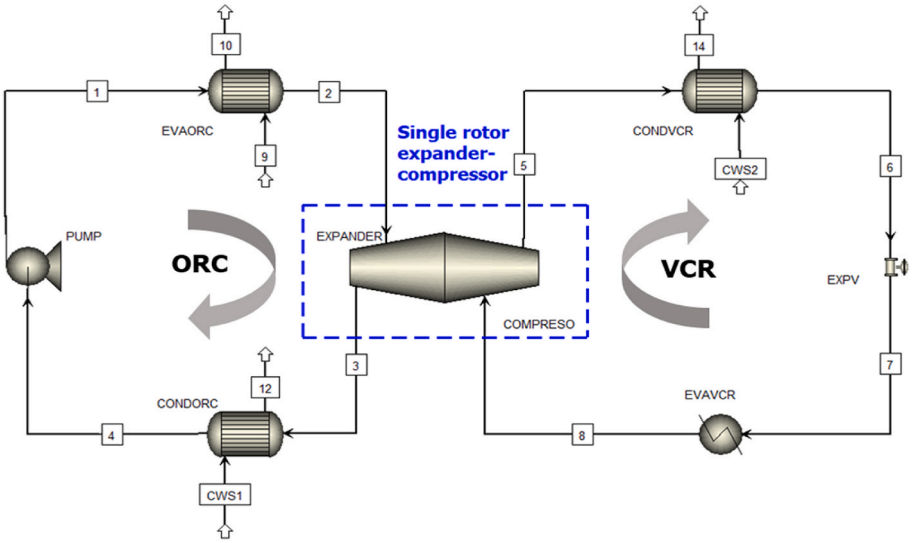

Fig. 3. Schematic diagram of the ORC-VCR system.

Table 2
Details of system components adopted from ASPEN Plus library.

Sr. No	Components	Abbreviation	ASPEN Plus model	Inputs
ORC				
1	Pump $\dot{W}_{ORC-pump} = \dot{m}_{ORC} \times (h_1 - h_4)$	PUMP	Pump	• Outlet pressure (5 bar–10 bar). • Pump efficiency, 75% [48].
2	Evaporator $Q_{eva,ORC} = \dot{m}_{ORC} \times (h_2 - h_1)$	EVAORC	HeatX	• Heating water temperature (95 °C) and mass flow rate (1 kg/s). • Working fluid at the evaporator outlet is saturated vapor ($x_{EVAORC} = 1$). • Minimum temperature approach (5 °C).
3	Expander $\dot{W}_{ORC,Exp} = \dot{m}_{ORC} \times (h_2 - h_3)$	EXPANDER	Turbine	• Isentropic efficiency, 80% [46]. • Displacement volume (15.7 cm^3). • Discharge pressure (condensation pressure) (1.227 bar–2.945 bar).
4	Condenser $Q_{cond,ORC} = \dot{m}_{ORC} \times (h_3 - h_4)$	CONDORC	HeatX	• Cooling water temperature (15 °C) and mass flow rate (1 kg/s). • Working fluid at the outlet of the condenser is saturated liquid ($x_{CONDORC} = 0$). • Minimum temperature approach (5 °C)
VCR				
1	Compressor $\dot{W}_{VCR,comp} = \dot{m}_{VCR} \times (h_5 - h_8)$	COMPRESO	Compr	• Expander output is fed to compressor as input ($\dot{W}_{EXPANDER} = \dot{W}_{COMPRESO}$). • Displacement volume (23 cm^3). • Isentropic efficiency, 80% [46].
2	Condenser $Q_{cond,VCR} = \dot{m}_{VCR} \times (h_5 - h_6)$	CONDVCR	HeatX	• Cooling water temperature (15 °C–40 °C) and mass flow rate (1 kg/s). • Working fluid at the outlet of the condenser is saturated liquid ($x_{CONDVCR} = 0$). • Minimum temperature approach (5 °C).
3	Expansion valve $h_6 = h_7$	EXPV	Valve	• VCR evaporation pressure (1.327 bar–3.496 bar).
4	Evaporator $Q_{eva,VCR} = \dot{m}_{VCR} \times (h_8 - h_7)$	EVAVCR	Heater	• Working fluid at the evaporator outlet is saturated vapor ($x_{EVAVCR} = 1$). • Minimum temperature approach (5 °C).

3. Results and discussion

3.1. Assessing the optimal side for the expander

Since the two sides of device have different amount of displaced volume, an investigation is performed to select the optimal side for the expansion and compression processes occurring in the ORC subsystem and VCR subsystem for given pair of refrigerants. Fig. 7(a) and (b) show the effect of ORC expander inlet pressure on VCR compressor discharge pressure for different condensation temperature of ORC and shaft speed of 1000 rpm, when displacement volume of expander is 15.7 cm^3 (small side) and 23 cm^3 (big side), respectively. This means that when the expansion process is on the small side, the default compression process is on the large side and vice versa. In Fig. 6 the critical pressure line refers to the critical pressure of the refrigerant used in the VCR subsystem which is R134a.

It can be seen in both scenarios that as expander inlet pressure increases, the compressor discharge pressure increases dramatically. Increasing the pressure at the inlet of the expander increases the power generated by the expander, which is finally fed to compressor of the VCR. Since the volume flow rate and the evaporation temperature ($T_{eva,VCR} = 0$ °C) of the VCR system are constants, the mass flow rate remains constant. Thus, only the discharge pressure of the compressor is free to increase when inlet pressure of expander increases. It is observed that the rise in discharge pressure of the compressor is steeper with increase in inlet pressure of the expander when expansion occurs in big side as compared to in small side. For instance, the discharge pressure is about 14.2 bar at an inlet pressure of 8 bar for a condensation temperature of 35 °C when expansion process takes place in small side, as shown in Fig. 7(a). On the other hand, under similar conditions the discharge pressure touches 108 bar (above critical point 40.59 bar of R134a) when expansion occurs in big side, which is approximately six time larger than the small side, as presented in Fig. 7(b).

Moreover, it is observed that increasing condensation temperature of the ORC reduces the discharge pressure of the compressor due to reduction in the power generated that being supplied by the expander to the compressor. In the case of small side, for a constant expander inlet pressure at 8 bar, the compressor discharge pressure decreases from 27.6 bar to 9.6 bar as $T_{cond,ORC}$ increases from 20 °C to 45 °C, respectively. This decrease is steeper in case of expansion in bigger side. From Fig. 5, it can be concluded that when bigger side acts as an expander, the increase in discharge pressure is steeper and most operating conditions are above critical pressure of refrigerant (VCR). Considering this fact, in this study the small side of the device is used as an expander while the big side is used as a compressor.

3.2. Effect of ORC evaporation temperature and shaft speeds

3.2.1. Effects on $Q_{eva,ORC}$ and $Q_{eva,VCR}$

Fig. 8 shows $Q_{eva,ORC}$ and $Q_{eva,VCR}$ of ORC and VCR under the variation of evaporation temperature when the single rotor expander-compressor speed varies from 500 to 3000 rpm. For a given speed, $Q_{eva,ORC}$ is increasing with the evaporation temperature of the ORC ($T_{eva,ORC}$) attributed to the increase in the mass flow rate of refrigerant in the ORC. As evaporation temperature of the ORC increases, the mass flow rate of refrigerant increases due to the increase in density at exit of evaporator of ORC as the vapor compressibility increases (see Eq. (1)). At the same time, latent heat of evaporation decreases as the evaporation pressure increases. Overall, the effect of increasing mass flow rate is more pronounced than the decrease in latent heat leading to an increase in $Q_{eva,ORC}$. It is obvious that $Q_{eva,ORC}$ is independent of the evaporation temperature of the VCR. At 500 rpm and regardless of $T_{eva,VCR}$, $Q_{eva,ORC}$ increases from 1.6 kW to 3.56 kW, an increase of 122%, when $T_{eva,ORC}$ increases from 62.5 °C to 89.7 °C. Similarly, at 3000 rpm, $Q_{eva,ORC}$ increases from 9.6 kW to 21.2 kW for the same $T_{eva,ORC}$ range. An increase in mass flow rate increases the power input to the compressor as the expander output power increases.

When $T_{eva,ORC}$ increased from 62.5 °C to 89.7 °C at 500 rpm, the work produces by the expander changed from 0.14 kW to 0.44 kW. At 3000 rpm, the expander work is 0.84 kW corresponding to $T_{eva,ORC} = 62.5$ °C and 2.65 kW corresponding to $T_{eva,ORC} = 89.7$ °C. An increase in the work supplied to compressor increases the condensation pressure at its outlet as discussed in previous section. As the condensing pressure of VCR increases, the vapor quality also increases after expansion. Thus, in the evaporator of VCR, a less amount of liquid refrigerant participates in the heat absorption process. Thus, $Q_{eva,VCR}$ at any given $T_{eva,VCR}$ decreases with increase in evaporation temperature of ORC as the mass flow rate of the VCR remains unchanged.

For 500 rpm and $T_{eva,VCR} = -20$ °C the maximum $Q_{eva,VCR}$ is 0.8 kW when $T_{eva,ORC}$ is 75 °C and the minimum is 0.3 kW at 89.7 °C. For the same speed, the maximum $Q_{eva,VCR}$ at $T_{eva,VCR} = 5$ °C is 0.82 kW when $T_{eva,ORC}$ is 62.75 °C and the minimum is 0.34 kW when 80.5 °C. Similarly, at 3000 rpm and $T_{eva,VCR} = -20$ °C the maximum $Q_{eva,VCR}$ is 5.15

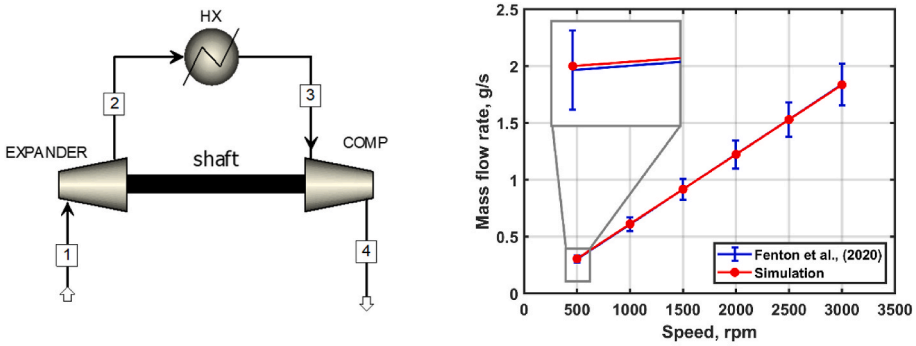

Fig. 5. Validation of a new single rotor expander-compressor device with experimental data of Fenton et al. [44] (a) system configuration, (b) comparison of mass flow rate.

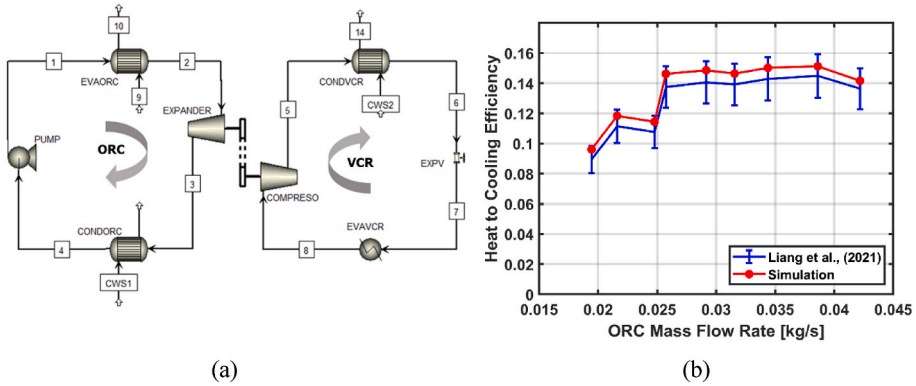

Fig. 6. (a) System configuration Liang et al. [36], (b) Comparison of current ORC-VCR model with experiment results in terms of ORC mass flow rate and heat to cooling efficiency.

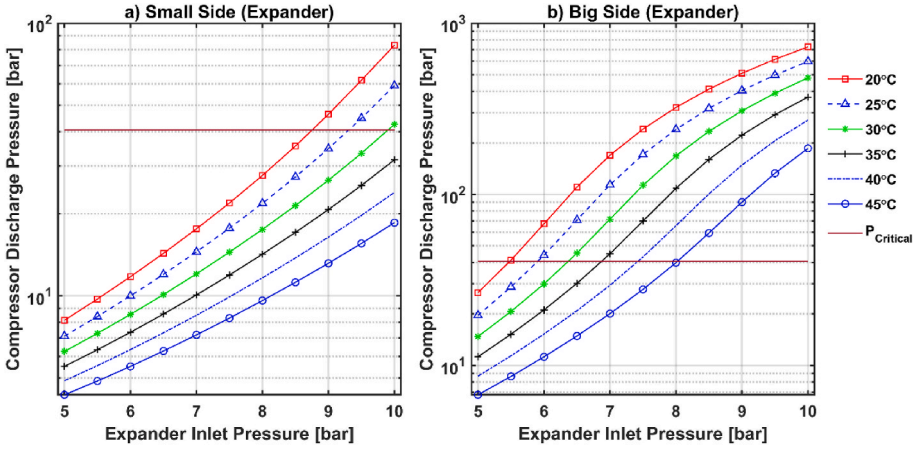

Fig. 7. Expander inlet pressure against ORC and VCR mass flow rates and compressor discharge pressure: (a) expander is the small side of the device, (b) expander is the big side of the device.

kW when $T_{eva,ORC}$ is 72.4 °C and the minimum is 1.19 kW at 89.7 °C. For the same speed, the maximum $Q_{eva,VCR}$ at $T_{eva,VCR}$ = 5 °C is 4.97 kW when $T_{eva,ORC}$ is 62.75 °C and the minimum is 2.05 kW when 80.5 °C. However, the overall maximum $Q_{eva,VCR}$ for the operating range under consideration is 5.38 kW at 3000 rpm, $T_{eva,ORC}$ = 62.75 °C and $T_{eva,VCR}$ = - 5 °C. The rotor speed plays a vital role and $Q_{eva,ORC}$ increases linearly with speed due to the increased volume displaced by the expander and compressor sides of the device. For 1000 rpm, 1500 rpm, 2000 rpm, 2500 rpm and 3000 rpm the average increase in $Q_{eva,ORC}$ and $Q_{eva,VCR}$ is 200%, 300%. 400%, and 500% compared to 500 rpm, respectively.

3.2.2. *Effects on* η_{H-C} *and* $\eta_{oval-ex}$

Fig. 9 presents the variation of heat-to-cooling efficiency (η_{H-C}) and overall exergy efficiency ($\eta_{oval-ex}$) of ORC-VCR system for different shaft speed and evaporation temperatures of the ORC and VCR. As seen in Fig. 8 the heat-to-cooling efficiency for all shaft speeds under consideration shows a decreasing trend with the increase in $T_{eva,ORC}$ which is

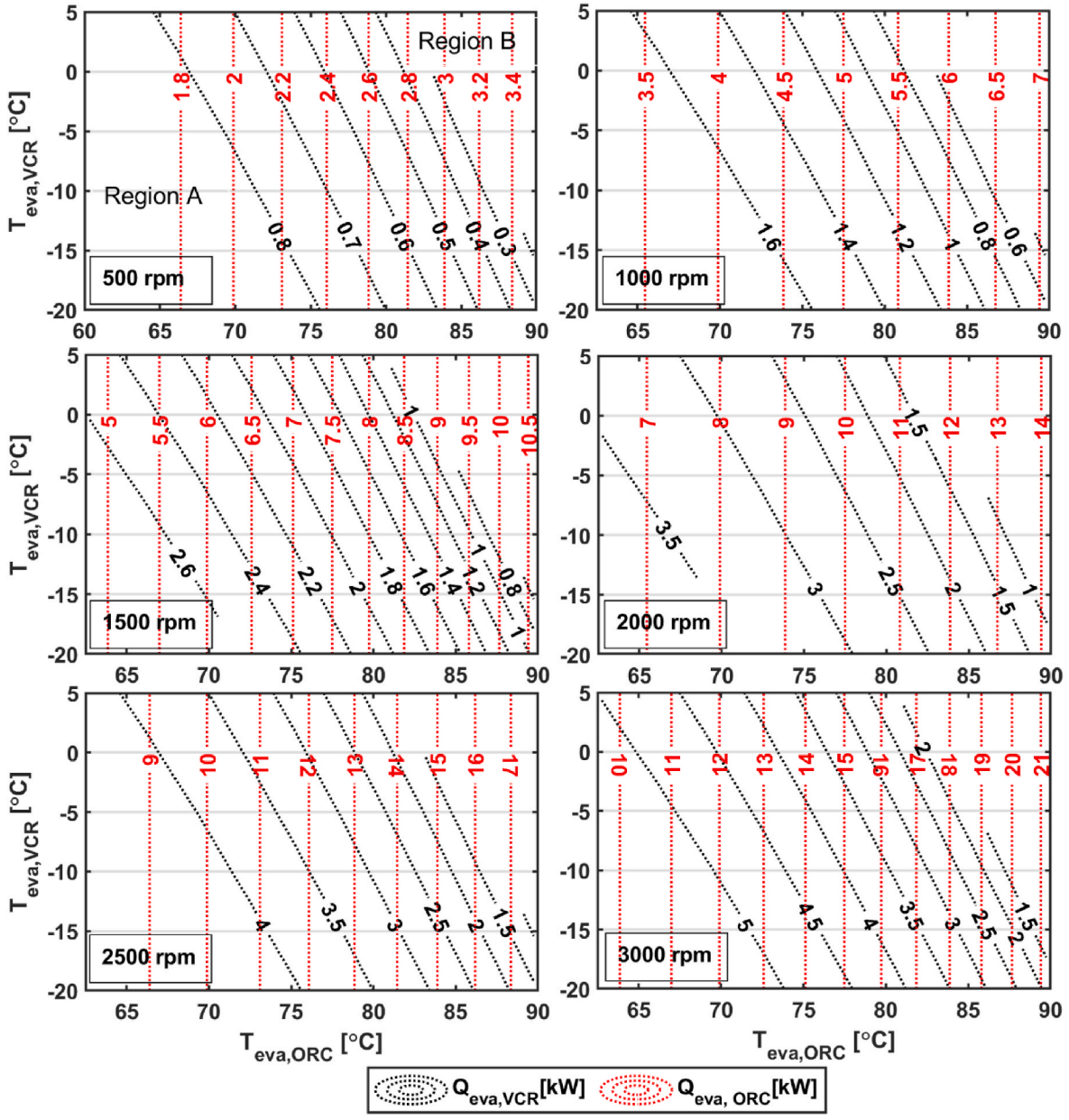

Fig. 8. Variation of $\mathbf{Q_{eva,ORC}}$ and $\mathbf{Q_{eva,VCR}}$ under the influence of evaporation temperatures of ORC and VCR for different speeds and $\mathbf{T_{cond,ORC}} = 20.5$ °C.

attributed to the decreasing trend of $Q_{eva,VCR}$. It can be seen that, at 500 rpm and $T_{eva,VCR} = -20$ °C, η_{H-C} varies between 40% and 9% when $T_{eva,ORC}$ increases from 72.4 °C to 89.7 °C. On the other hand, at $T_{eva,VCR} = 5$ °C, η_{H-C} corresponds to $T_{eva,ORC} = 62.7$ °C is 51% and that to $T_{eva,ORC} = 80.5$ °C is 6%. It is found that the overall highest η_{H-C} of 56% is obtained at $T_{eva,ORC} = 62.75$ °C and $T_{eva,VCR} = -5$ °C. Furthermore, the rotor speed does not influence the heat-to-cooling efficiency showing the same magnitude for all speeds under consideration.

Also, Fig. 9 shows the variation of the overall exergy efficiency of the system under different T_{eva} of ORC and VCR for different shaft speeds. The overall exergy efficiency shows a decreasing trend for all speeds under consideration. This is attributed to the increased exergy destruction $\dot{E}_{cooling}$ across the evaporator of VCR and exergy destruction $\dot{E}_{in}$ in pump and evaporator of ORC. $\dot{E}_{in}$ increases as exergy flow of stream 2 increases dramatically compared to the increase in exergy flow of stream 1 with an increase in $T_{eva,ORC}$. Moreover, exergy flow in stream 7 after expansion valve decreases leading to increase in $\dot{E}_{cooling}$ with $T_{eva,ORC}$. However, exergy destruction in the ORC sub-cycle is greater than the one in the VCR sub-cycle. Thus, increasing $T_{eva,ORC}$ increases $\eta_{oval-ex}$ for all speeds. It is observed, at 500 rpm, $\eta_{oval-ex}$ varies between 11% and 60% when $T_{eva,ORC}$ increase from 72.4 °C to 89.7 °C at $T_{eva,VCR} = -20$ °C. On the other hand, at $T_{eva,VCR} = 5$ °C, $\eta_{oval-ex}$ corresponding to $T_{eva,ORC} = 62.7$ °C is 37% and that to of $T_{eva,ORC} = 80.5$ °C is 7%. It is observed that the overall highest $\eta_{oval-ex}$ of 63% is obtained at $T_{eva,ORC} = 62.75$ °C and $T_{eva,VCR} = -5$ °C. Furthermore, as seen in Fig. 8, the overall exergy efficiency is independent of the change of shaft speed.

In Figs. 8 and 9, there are two blank regions as indicated by Region A and Region B. For region A, at lower $T_{eva,ORC}$, the expander produces less power, which can be enough to run the compressor at high $T_{eva,VCR}$, but at $T_{eva,VCR}$, the difference between the compressor discharge stream temperature and the ambient temperature reaches the minimum temperature approach, which was set to 5 °C in the condenser of the VCR, as mentioned in Table 2. Thus, the complete condensation is not achieved in the condenser leading to two-phase entry of the refrigerant at the entry of the expansion device. Under this circumstance, model do not converge and fail to generate reliable results. For Region B, when the

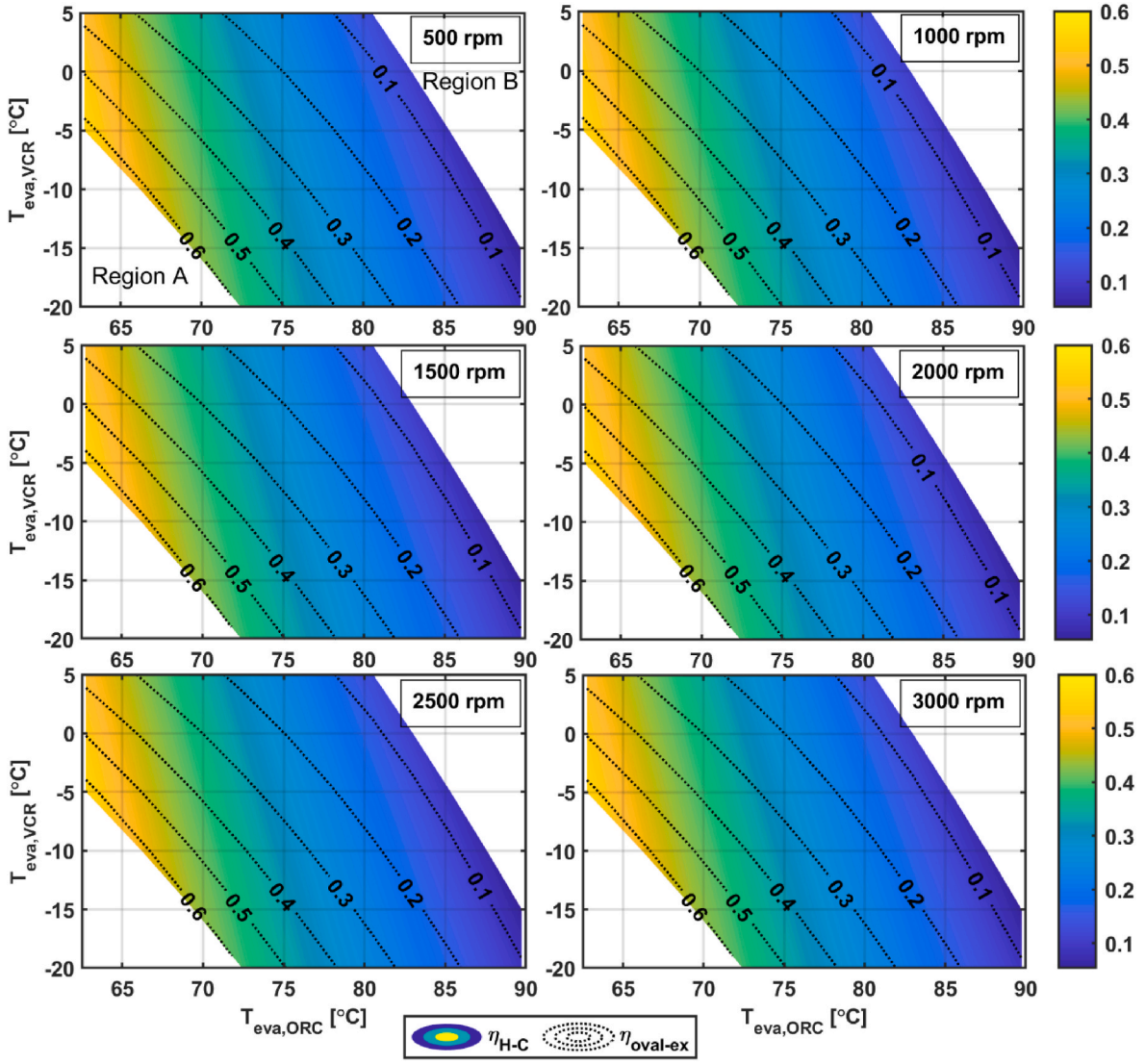

Fig. 9. Variation of η_{H-C} and $\eta_{oval-ex}$ under the influence of evaporation temperatures of ORC and VCR for different speeds and $T_{cond,ORC}$ = 20.5 °C.

output power of the expander started increasing, the compressor discharge pressure increased to the point where the compressor discharge pressure reached the critical pressure (for R134a, 40.593 bar). Thus, the condensation process was not completed. Consequently, the model does not converge and not able to produce cooling effects under these conditions.

3.3. Effect of ORC condensation temperature

3.3.1. Effects on $Q_{eva,ORC}$ and $Q_{eva,VCR}$

Fig. 10 shows the effects of condensation temperature of ORC $T_{cond,ORC}$ on the $Q_{eva,ORC}$ and the $Q_{eva,VCR}$. Increasing $T_{cond,ORC}$ resulted in a slight decrease in $Q_{eva,ORC}$ and that can be attributed to increase in enthalpy at the evaporator inlet of ORC due to the increase in liquid refrigerant temperature at the evaporator inlet. Therefore, the enthalpy difference across the evaporator of ORC decreases because the enthalpy at its outlet is constant (assumption 3). $Q_{eva,ORC}$ decreases from 2.75 kW to 2.36 kW for 500 rpm when $T_{cond,ORC}$ increases from 20 °C to 45 °C. At 3000 rpm, $Q_{eva,ORC}$ is 16.51 kW at $T_{cond,ORC}$ = 20 °C and drops to 14.17 kW at $T_{cond,ORC}$ = 45 °C. Furthermore, increasing $T_{cond,ORC}$ increases the outlet pressure of the expander which reduces the power generated by the expander of ORC. This reduces the input power to the compressor of VCR subsystem reduces. At 500 rpm, the expander work is 0.32 kW at $T_{cond,ORC}$ = 20 °C and drop to 0.17 kW at $T_{cond,ORC}$ = 45 °C. When $T_{cond,ORC}$ increases from 20 °C to 45 °C, the expander work decreases from 1.92 kW to 1.02 kW for 3000 rpm.

The outlet pressure of the compressor (condensation pressure of VCR) decreases as the work supplied to compressor decreases. This results in a decrease in vapor quality after expansion which makes more liquid refrigerant available for the heat absorption process in the evaporator of VCR at the same evaporation pressure. Consequently, $Q_{eva,VCR}$ increases as the condensation temperature of the ORC increases, as presented in Fig. 9. For 500 rpm, at $T_{eva,VCR}$ = −20 °C the maximum $Q_{eva,VCR}$ is 0.79 kW when $T_{cond,ORC}$ is 30 °C and the minimum is 0.66 kW at 20 °C. For the same speed, the maximum $Q_{eva,VCR}$ at $T_{eva,VCR}$ = 5 °C is 0.69 kW when $T_{cond,ORC}$ is 40 °C and the minimum is 0.62 kW when $T_{cond,ORC}$ is 35 °C. Similarly, at 3000 rpm and $T_{eva,VCR}$ = −20 °C the maximum $Q_{eva,VCR}$ is 4.75 kW when $T_{cond,ORC}$ is 30 °C and the minimum is 3.98 kW at $T_{cond,ORC}$ = 20 °C. For the same speed, the maximum $Q_{eva,VCR}$ at $T_{eva,VCR}$ = 5 °C is 4.58 kW when $T_{cond,ORC}$ is 45 °C and minimum is 3.74 kW when $T_{cond,ORC}$ = 35 °C. However, the overall maximum $Q_{eva,VCR}$ for the operating ranges under consideration is 4.75 kW at 3000 rpm, $T_{con,ORC}$ = 30 °C and $T_{eva,VCR}$ = −20 °C.

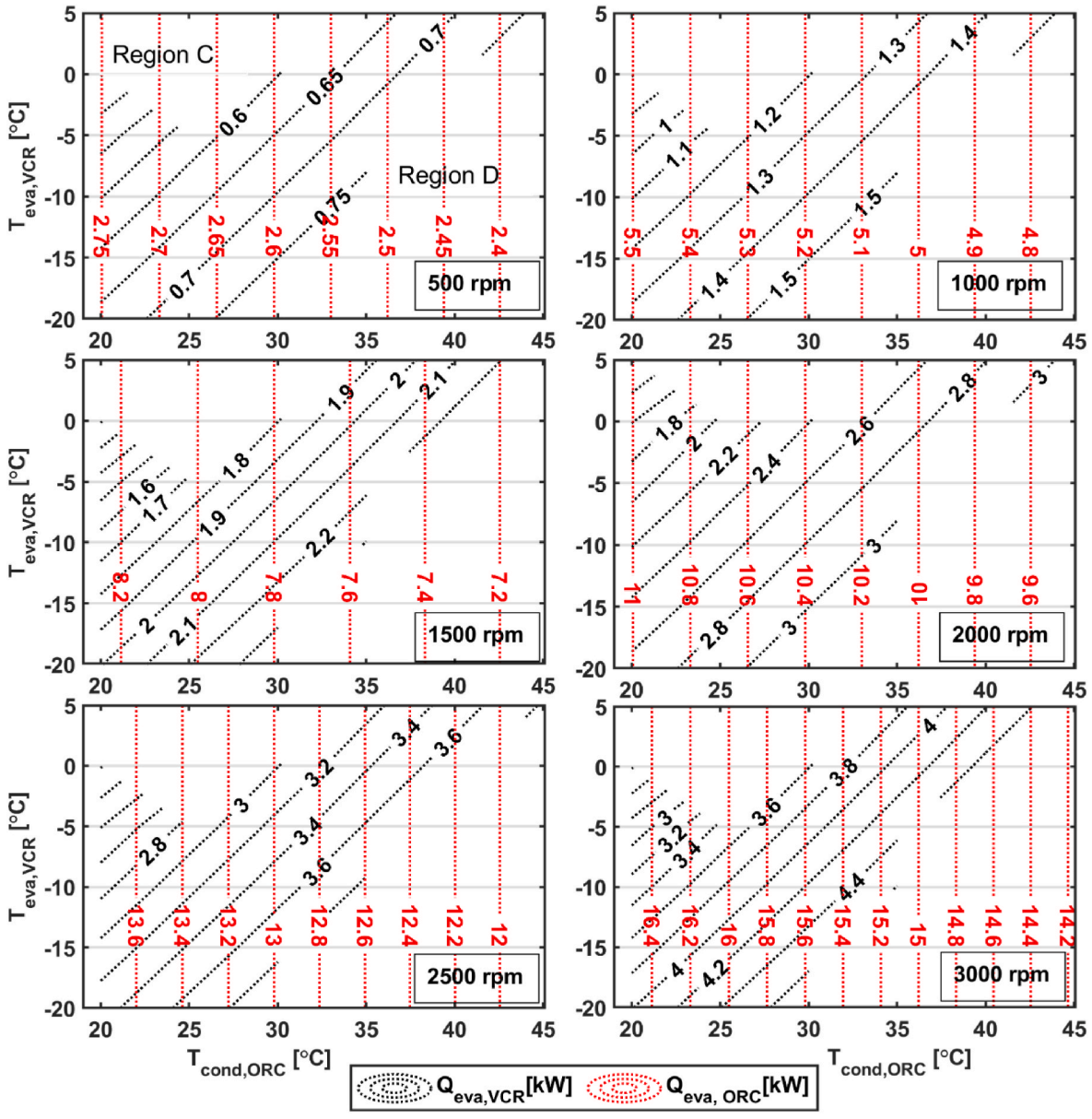

Fig. 10. Variation of $\mathbf{Q_{eva,ORC}}$ and $\mathbf{Q_{eva,VCR}}$ under the influence of condensation temperatures of ORC and VCR for different speeds and evaporation temperature of ORC is 80.53 °C.

3.3.2. *Effects of* $\mathbf{T_{cond,ORC}}$ *on* η_{H-C} *and* $\eta_{oval-ex}$

Fig. 11 illustrate the distribution of the heat-to-cooling efficiency and the overall exergy efficiency under variation of $T_{cond,ORC}$ and $T_{eva,VCR}$ for different shaft speeds. The heat-to-cooling efficiency increases with the increase of condensation temperature of ORC and the dependence is pronounced at higher condensation temperatures. On the other hand, the heat-to-cooling efficiency shows a decreasing trend with respect to the increase in the evaporation temperature of VCR. This is described by the fixed condensation temperature and constant shaft speed, the cooling capacity, $Q_{eva,VCR}$, decreases when the VCR evaporation temperature increases. Since the heat absorbed by the ORC evaporator is almost constant at different condensing temperature, any increase in cooling capacity will increase the heat-to-cooling efficiency. As can be seen, at 500 rpm, η_{H-C} varies between 24% and 30% while $T_{eva,VCR} = -20$ °C as $T_{cond,ORC}$ increases from 20 °C to 45 °C at. On the other hand, at $T_{eva,VCR} = 5$ °C, η_{H-C} corresponds to $T_{cond,ORC} = 40$ °C is 28% and that corresponds to $T_{cond,ORC} = 45$ °C is 32%.

It is found that the overall highest η_{H-C} of 32% is obtained at $T_{cond,ORC} = 45$ °C and $T_{eva,VCR} = 5$ °C. Furthermore, the rotor speed does not influence the heat-to-cooling efficiency showing the same magnitude for all speeds under consideration.

The overall exergy efficiency increases with the increase of $T_{cond,ORC}$ as shown in Fig. 11, due to a decrease in power supplied to the compressor, which in turn reduces the compressor discharge pressure. As a result, the exergy destruction in the expansion valve is reduced leading to an increase in $Q_{eva,VCR}$ and thus overall exergy efficiency. It is observed that, at 500 rpm, $\eta_{oval-ex}$ varies between 33% and 39% while $T_{eva,VCR} = -20$ °C as $T_{cond,ORC}$ increases from 20 °C to 45 °C, respectively. On the other hand, at $T_{eva,VCR} = 5$ °C, $\eta_{oval-ex}$ corresponding to $T_{cond,ORC} = 40$ °C is 14% and that of $T_{cond,ORC} = 45$ °C is 16%. It is found that the overall highest $\eta_{oval-ex}$ of 39% is obtained at $T_{cond,ORC} = 30$ °C and $T_{eva,VCR} = -20$ °C.

In Figs. 10 and 11, there are two blank regions indicated by Region C and Region D. For Region C, at lower $T_{cond,ORC}$ and higher $T_{eva,VCR}$ the output power of the expander was the highest which led to increasing in the compressor discharge pressure and temperature. Reaching the

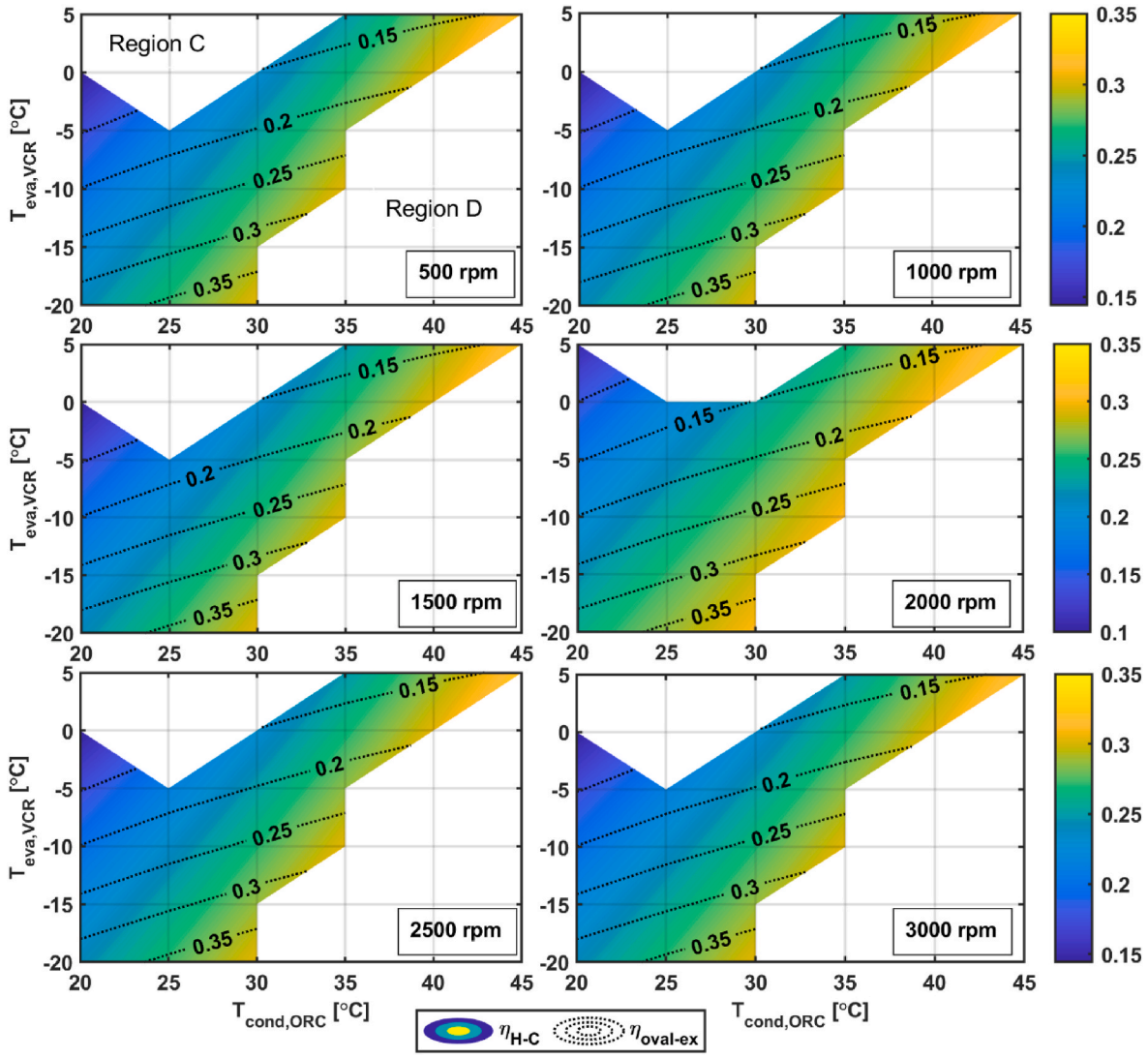

Fig. 11. Variation of η_{H-C} and $\eta_{oval-ex}$ under the influence of condensation temperatures of ORC and VCR for different speeds.

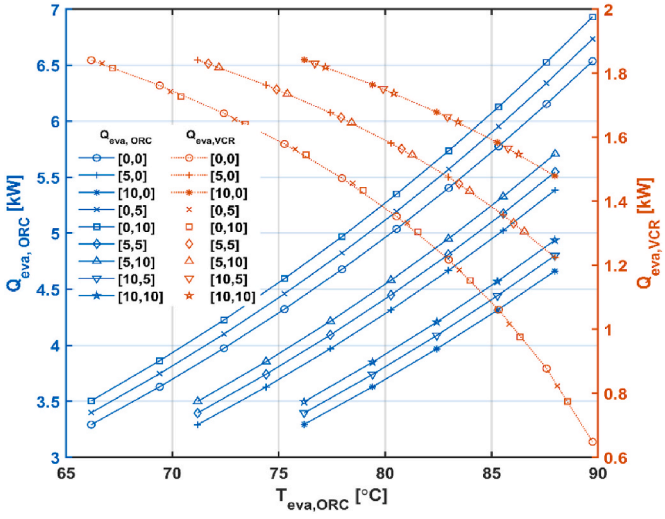

Fig. 12. Influence of the degree of superheating (ΔT_{sup}) and degree of subcooling (ΔT_{sub}) on $\mathbf{Q_{eva,ORC}}$ and $\mathbf{Q_{eva,VCR}}$. In legends, square parenthesis indicates [ΔT_{sup}, ΔT_{sub}].

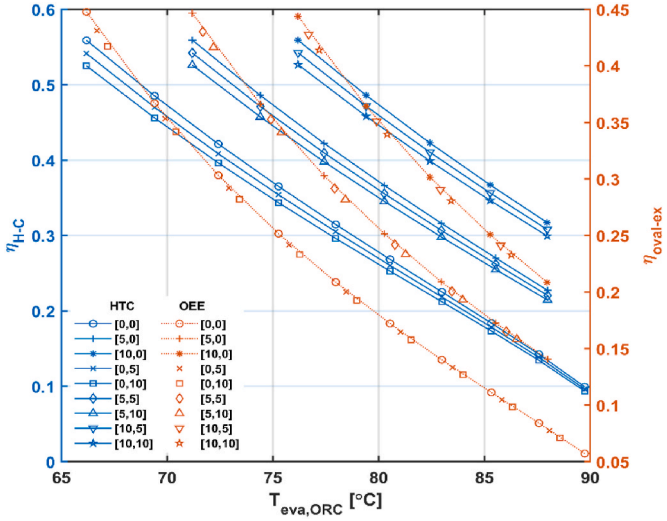

Fig. 13. Influence of the degree of superheating (ΔT_{sup}) and degree of subcooling (ΔT_{sub}) on η_{H-C} and $\eta_{oval-ex}$. In legends, square parenthesis indicates [ΔT_{sup}, ΔT_{sub}].

critical pressure or temperature will lead the refrigerant not to fully condensed. Consequently, the model of system will terminate without producing cooling effects at high $T_{eva,VCR}$. For Region D, when $T_{cond,ORC}$ start increasing the output power of the expander will decrease which led to decrease in the compressor discharge pressure. Since the ORC subsystem and VCR subsystem work under the same ambient conditions the condensation temperature should not be lower than $T_{cond,ORC}$. Thus, the system was not able to produce cooling effects.

3.4. Effect of degree of superheating and subcooling

Fig. 12 shows the effect of ΔT_{sup} and ΔT_{sub} of the ORC subsystem on the $Q_{eva,ORC}$ and $Q_{eva,VCR}$ at $T_{eva,VCR} = 0$ °C, and speed shaft of 1000 rpm. ΔT_{sup} and ΔT_{sub} varies from 0 °C to 10 °C, and the variation led to 9 sets of conditions.

For [0,0] set, $T_{eva,ORC}$ is varied from 66.19 °C to 89.74 °C at a constant $T_{cond,ORC}$ of 35 °C. The results showed, increasing ΔT_{sup} did not increase $Q_{eva,ORC}$ or $Q_{eva,VCR}$. However, increasing ΔT_{sub} led to increase in $Q_{eva,ORC}$ which can be seen by comparing the three sets: [0,0], [0,5], and [0,10]. $Q_{eva,ORC}$ increased by 6.4% when ΔT_{sub} increased from 0 °C to 10 °C at constant $\Delta T_{sup} = 0$ °C. ΔT_{sub} has no effect on $Q_{eva,VCR}$ as it illustrated [5,5,5,10] are overlapped. Similarly, Fig. 11 presents the variation of both heat-to-cooling efficiency and overall exergy efficiency for the same assumptions applied to Fig. 13.

Results show that increasing ΔT_{sup} does not increase heat-to-cooling efficiency or the overall exergy efficiency. However, increasing ΔT_{sub} resulted in a decrease in heat-to-cooling efficiency. When ΔT_{sub} increases from 0 °C to 10 °C at constant $\Delta T_{sup} = 0$ °C, the heat-to-cooling efficiency decreases by 6.4%. This decrease is associated with an increase in $Q_{eva,ORC}$ while $Q_{eva,VCR}$ remains constant. ΔT_{sub} has no effect on overall exergy efficiency as it illustrated [5,5,5,10] are overlapped.

4. Conclusions

The potential of a new single rotor expander-compressor device in cooling application through combined vapor compression refrigeration (VCR) cycle and an organic Rankine cycle (ORC) is investigated. The thermal performance evaluation is carried out to study the influence of evaporation temperature of ORC (62.75 °C–89.7 °C) and VCR (−20 °C–5 °C), condensation temperature of ORC (20 °C–45 °C) and speed (500–3000 rpm) at constant hot source (water) temperature of 95 °C. It is observed that.

- The rise in discharge pressure of the compressor is sensitive to the displaced volume on each side and is more pronounce with increase in inlet pressure of the expander when the expansion process occurs in side B, which has a larger displacement than side A. Moreover, the high condensation temperature in the ORC lowers discharge pressure of the compressor.
- With increasing evaporator temperature of ORC from 62.5C to 89.7C, the refrigerating effect, $Q_{eva,ORC}$ increases from 1.6 kW to 3.56 kW and 9.6 kW–21.2 kW, almost increment of 120%, when speed is 500 rpm and 3000 rpm, respectively. Furthermore, at 500 rpm and $T_{eva,VCR} = -20$ °C, heat-to-cooling efficiency and exergy efficiency varies between 40% to 9% and 37%–7% when $T_{eva,ORC}$ increases from 72.4 °C to 89.7 °C, respectively. On the other hand, at $T_{eva,VCR} = 5$ °C, heat-to-cooling efficiency and exergy efficiency corresponds to $T_{eva,ORC} = 62.7$ °C is 51% and 37% and that to $T_{eva,ORC} = 80.5$ °C is 6% and 7%, respectively.
- Similarly, with increasing condensation temperature of ORC from 20 °C to 30 °C, the refrigerating effect, $Q_{eva,ORC}$ increases from 0.66 kW to 0.79 kW and 3.98 kW–4.75 kW, when speed is 500 rpm and 3000 rpm, respectively. Furthermore, at 500 rpm and $T_{eva,VCR} = -20$ °C, heat-to-cooling efficiency and exergy efficiency varies between 24% to 30% and 30%–39% when $T_{cond,ORC}$ increases from 20 °C to 45 °C, respectively. On the other hand, at $T_{eva,VCR} = 5$ °C, heat-to-cooling efficiency and exergy efficiency corresponds to $T_{cond,ORC} = 40$ °C is 28% and 14% and that to $T_{cond,ORC} = 45$ °C is 32% and 16%, respectively.
- In general, the highest levels of cooling effect, heat-to-cooling efficiency, and exergy efficiency achieved were 5.38 kW, 56%, and 63%, respectively. These values were obtained when the evaporation temperature of ORC and VCR was set to 62.75 °C and −5 °C, respectively, and the condensation temperature of ORC was set to 20.5 °C. The cooling effect showed a linear increase with rotor speed, while the heat-to-cooling efficiency and exergy efficiency remained unaffected by changes in rotor speed.

The numerical results implies that the new single rotor expander-compressor device performs well in a combined organic Rankine cycle and vapor compression refrigeration cycle, demonstrating reliable performance. However, further numerical analysis of the combined cycle using new device is essential from the point of second law efficiency at component level and, as well as the cost and environmental impact of considering the combination different eco-friendly refrigerants in both ORC and VCR. Moreover, conducting experimental investigations is recommended to validate the device's stability and suitability for cooling applications.

Declaration of competing interest

The authors declare that they have no known competing financial interests or personal relationships that could have appeared to influence the work reported in this paper.

Data availability

Data will be made available on request.

Acknowledgement

This work was mainly supported by EPSRC in the UK through the grant EP/V042033/1 and EP/T022701/1, but also benefited from other EPSRC grants EP/W027593/1, EP/V030515/1, EP/P028829/1, EP/N020472/1, EP/R003122/1, EP/W027593/1, and EP/N005228/1. Saif Alshammari acknowledges the financial support for his PhD from Jouf university, Saudi Arabia, managed by the cultural bureau in Saudia Arabia embassy within the UK.

Nomenclature

Subscripts

C	Compressor
compr	Compressor
Cond	Condenser
Cond	Condensation
COP	Coefficient of performance
CWS	Cooling Water Stream

E	Exergy destruction, kW
E	Expander
Eva	Evaporation
h	Enthalpy, kj/kg
H	Higher
H–C	Heat to cooling
HeatX	Heat Exchanger
L	Lower
$\dot{m}$	Mass flow rate, kg/s
o	Dead state
ORC	Organic Rankine cycle
P	Pressure, bar
$\dot{Q}$	Rate of heat, kW
s	Specific entropy, $kJ/kg^{-1}K^{-1}$
sub	Subcooled
sup	Superheated
T	Temperature, °C
V	Displacement volume, cm^3/rev
VCR	Vapor compression refrigeration cycle
$\dot{W}$	Power, kW

Greek Letters

ρ	Density, kg/ m^3
η	Thermal efficiency
ω	shaft speed, rpm

References

[1] EPA. Inventory of U.S. Greenhouse gas emissions and sinks: 1990-2020. U.S. Environmental Protection Agency; 2022. EPA 430-R-22-003.
[2] Is the climate warming?. Available, https://royalsociety.org/topics-policy/projects/climate-change-evidence-causes/question-1/; 2020.
[3] Agency IE. The Future of Cooling: opportunities for energy-efficient air conditioning. OECD Publishing; 2018.
[4] Peters T. A cool world defining the energy conundrum of cooling for all. UK: University of Birmingham; 2018.
[5] Agreement P. Paris agreement. In: Report of the conference of the parties to the united nations framework convention on climate change (21st session, 2015: Paris). Retrived december, vol. 4. HeinOnline; 2015. 2017.
[6] She X, Yin Y, Xu M, Zhang X. A novel low-grade heat-driven absorption refrigeration system with LiCl–H2O and LiBr–H2O working pairs. Int J Refrig 2015;58:219–34.
[7] Tchanche BF, Lambrinos G, Frangoudakis A, Papadakis G. Low-grade heat conversion into power using organic Rankine cycles - a review of various applications. Renewable & Sustainable Energy Reviews, Review Oct 2011;15(8):3963–79 (in English).
[8] Ping X, Yang F, Zhang H, Xing C, Yu M, Wang Y. Investigation and multi-objective optimization of vehicle engine-organic Rankine cycle (ORC) combined system in different driving conditions. Energy 2023;263.
[9] Saedi A, Jahangiri A, Ameri M, Asadi F. Feasibility study and 3E analysis of blowdown heat recovery in a combined cycle power plant for utilization in Organic Rankine Cycle and greenhouse heating. Energy 2022;260.
[10] Chen C, Witte F, Tuschy I, Kolditz O, Shao H. Parametric optimization and comparative study of an organic Rankine cycle power plant for two-phase geothermal sources. Energy 2022;252.
[11] Hung T-C, Shai T, Wang SK. A review of organic Rankine cycles (ORCs) for the recovery of low-grade waste heat. Energy 1997;22(7):661–7.
[12] yamamoto T, Furuhata T, Arai N, Mori K. Design and testing of the organic rankine cycle. Energy 2001;26:239–51.
[13] Li Y-R, Wang X-Q, Li X-P, Wang J-N. Performance analysis of a novel power/refrigerating combined-system driven by the low-grade waste heat using different refrigerants. Energy 2014;73:543–53.
[14] Li H, Bu X, Wang L, Long Z, Lian Y. Hydrocarbon working fluids for a Rankine cycle powered vapor compression refrigeration system using low-grade thermal energy. Energy Build 2013;65:167–72.
[15] Kim KH, Perez-Blanco H. Performance analysis of a combined organic Rankine cycle and vapor compression cycle for power and refrigeration cogeneration. Appl Therm Eng 2015;91:964–74.
[16] Nasir MT, Kim KC. Working fluids selection and parametric optimization of an Organic Rankine Cycle coupled Vapor Compression Cycle (ORC-VCC) for air conditioning using low grade heat. Energy Build 2016;129:378–95.
[17] Saleh B. Energy and exergy analysis of an integrated organic Rankine cycle-vapor compression refrigeration system. Appl Therm Eng 2018;141:697–710.
[18] Xia X, Liu Z, Wang Z, Sun T, Zhang H. Multi-layer performance optimization based on operation parameter-working fluid-heat source for the ORC-VCR system. Energy 2023;272:127103.
[19] Sherwani AF, Tiwari D. Exergy, economic and environmental analysis of organic Rankine cycle based vapor compression refrigeration system. Int J Refrig 2021;126:259–71.
[20] Park B-S, Usman M, Imran M, Pesyridis A. Review of organic rankine cycle experimental data trends. Energy Convers Manag 2018;173:679–91.
[21] Askari-Asli Ardeh E, Loni R, Najafi G, Ghobadian B, Bellos E, Wen D. Exergy and economic assessments of solar organic Rankine cycle system with linear V-Shape cavity. Energy Convers Manag 2019;199.
[22] Ziółkowski P, et al. Different design aspects of an Organic Rankine Cycle turbine for electricity production using a geothermal binary power plant. Energy Convers Manag 2021;246.
[23] Rijpkema J, Andersson SB, Munch K. Experimental study of an organic Rankine cycle with R1233zd(E) for waste heat recovery from the coolant of a heavy-duty truck engine. Energy Convers Manag 2021;244.
[24] Dai Y, Wang J, Gao L. Parametric optimization and comparative study of organic Rankine cycle (ORC) for low grade waste heat recovery. Energy Convers Manag 2009;50(3):576–82.
[25] Liu L, Zhu T, Ma J. Working fluid charge oriented off-design modeling of a small scale Organic Rankine Cycle system. Energy Convers Manag 2017;148:944–53.
[26] Shao L, Zhu J, Meng X, Wei X, Ma X. Experimental study of an organic Rankine cycle system with radial inflow turbine and R123. Appl Therm Eng 2017;124:940–7.
[27] Miao Z, Xu J, Zhang K. Experimental and modeling investigation of an organic Rankine cycle system based on the scroll expander. Energy 2017;134:35–49.
[28] Escalante ESR, Balestieri JAP, de Carvalho JA. The organic Rankine cycle: a promising technology for electricity generation and thermal pollution mitigation. Energy 2022;247.
[29] Salim MS, Kim M-H. Multi-objective thermo-economic optimization of a combined organic Rankine cycle and vapour compression refrigeration cycle. Energy Convers Manag 2019;199.
[30] Prigmore D, Barber R. Cooling with the sun's heat Design considerations and test data for a Rankine Cycle prototype. Sol Energy 1975;17(3):185–92.
[31] Lior N. Solar energy and the steam Rankine cycle for driving and assisting heat pumps in heating and cooling modes. Energy Convers 1977;16(3):111–23.
[32] Wang H, Peterson R, Herron T. Design study of configurations on system COP for a combined ORC (organic Rankine cycle) and VCC (vapor compression cycle). Energy 2011;36(8):4809–20.
[33] Chahartaghi M, Einanlou M, Hashemian SM. Energy and exergy analyses of a combined cooling, heating and power system with prime mover of phosphoric acid fuel cell with organic Rankine cycle. Appl Therm Eng 2021;193:116989.
[34] Aphornratana S, Sriveerakul T. Analysis of a combined Rankine–vapour–compression refrigeration cycle. Energy Convers Manag 2010;51(12):2557–64.
[35] Mahmoudan A, Samadof P, Sadeghzadeh M, Jalili M, Sharifpur M, Kumar R. Thermodynamic and exergoeconomic analyses and performance assessment of a new configuration of a combined cooling and power generation system based on ORC–VCR. J Therm Anal Calorim 2021;145:1163–89.

[36] Liang Y, Mckeown A, Yu Z, Alshammari SFK. Experimental study on a heat driven refrigeration system based on combined organic Rankine and vapour compression cycles. Energy Convers Manag 2021;234:113953.
[37] Liang Y, Yu Z, Li W. A waste heat-driven cooling system based on combined organic Rankine and vapour compression refrigeration cycles. Appl Sci 2019;9(20):4242.
[38] Wang H, et al. Performance of a combined organic Rankine cycle and vapor compression cycle for heat activated cooling. Energy 2011;36(1):447–58.
[39] Garland SD, Noall J, Bandhauer TM. Experimentally validated modeling of a turbo-compression cooling system for power plant waste heat recovery. Energy 2018;156:32–44.
[40] Grauberger A, Young D, Bandhauer T. Experimental validation of an organic rankine-vapor compression cooling cycle using low GWP refrigerant R1234ze (E). Appl Energy 2022;307:118242.
[41] Igobo ON, Davies PA. Review of low-temperature vapour power cycle engines with quasi-isothermal expansion. Energy 2014;70:22–34.
[42] Kim YM, D K S, J H L. A scroll expander with heating structure and their systems. In: Presented at the international compressor engineering conference; 2004. Purdue, July 12-15, 2004, https://docs.lib.purdue.edu/icec/1635.
[43] Jiang H, et al. Performance assessment of an organic Rankine–Vapor compression cycle (ORC-VCR) for Low-Grade compression heat recovery. Energy Convers Manag 2023;275:116492.
[44] J. Fenton, J. Subert, K. Hinchliffe, G. Bianchi, and S. Tassou, "Air cycle feasibility using a novel, single rotor compander for refrigeration and heating," in IIR international rankine 2020 conference-heating, Cooling and Power Generation, Glasgow, UK..
[45] Subert J, Fenton JP, Hinchliffe K, Arbon IM. Design optimization and test of the novel FeTu 'compander', utilising organic fluids within a closed cycle for HVACR applications. IOP Conf Ser Mater Sci Eng 2021;1180(1).
[46] Zhang Y, et al. The roticulating concept air compressor: experimental and numerical investigation. In: IOP conference series: materials science and engineering. vol. 604. IOP Publishing; 2019, 012070. 1.
[47] AspenTech. *AspenPlus Software* Available, https://www.aspentech.com/; 2022.
[48] Saleh B. Parametric and working fluid analysis of a combined organic Rankine-vapor compression refrigeration system activated by low-grade thermal energy. J Adv Res 2016;7(5):651–60.
[49] Kadam ST, et al. Thermo-economic and environmental assessment of hybrid vapor compression-absorption refrigeration systems for district cooling. Energy 2022;243:122991.